



Universiteit
Leiden
The Netherlands

Interpulse phase corrections for unbalanced pseudo-continuous arterial spin labeling at high magnetic field

Hirschler, L.; Debacker, C.S.; Voiron, J.; Kohler, S.; Warnking, J.M.; Barbier, E.L.

Citation

Hirschler, L., Debacker, C. S., Voiron, J., Kohler, S., Warnking, J. M., & Barbier, E. L. (2018). Interpulse phase corrections for unbalanced pseudo-continuous arterial spin labeling at high magnetic field. *Magnetic Resonance In Medicine*, 79(3), 1314-1324. doi:10.1002/mrm.26767

Version: Publisher's Version

License: [Licensed under Article 25fa Copyright Act/Law \(Amendment Taverne\)](#)

Downloaded from: <https://hdl.handle.net/1887/4107557>

Note: To cite this publication please use the final published version (if applicable).

Interpulse Phase Corrections for Unbalanced Pseudo-Continuous Arterial Spin Labeling at High Magnetic Field

Lydiane Hirschler,^{1,2,3} Clément S. Debacker,^{1,2,3} Jérôme Voiron,³ Sascha Köhler,³ Jan M. Warnking ^{1,2} and Emmanuel L. Barbier^{1,2*}

Purpose: To evaluate a prescan-based radiofrequency phase-correction strategy for unbalanced pseudo-continuous arterial spin labeling (pCASL) at 9.4 T in vivo and to test its robustness toward suboptimal shim conditions.

Methods: Label and control interpulse phases were optimized separately by means of two prescans in rats. The mean perfusion as well as the interhemispherical symmetry were measured for several phase combinations (optimized versus theoretical phases) to evaluate the correction quality. Interpulse phases were also optimized under degraded shim conditions (i.e., up to four times the study shim values) to test the strategy's robustness.

Results: For all tested shim conditions, the full arterial spin labeling (ASL) signal could be restored. Without any correction, the relative ASL signal was $1.4 \pm 1.7\%$. It increased to $3.6 \pm 1.4\%$ with an optimized label phase and to $5.3 \pm 1.2\%$ with optimized label and control phases. Moreover, asymmetry between brain hemispheres, which could be as high as 100% without phase optimization, was dramatically reduced to $1 \pm 3\%$ when applying optimized label and control phases.

Conclusions: Pseudo-continuous ASL at high magnetic field is very sensitive to shim conditions. Label and control radiofrequency phase optimization based on prescans robustly maximizes the ASL signal obtained with unbalanced pCASL and minimizes the asymmetry between hemispheres. **Magn Reson Med 79:1314–1324, 2018. © 2017 International Society for Magnetic Resonance in Medicine.**

Key words: unbalanced pseudo-continuous arterial spin labeling; interpulse phase optimization; perfusion; 9.4 T; preclinical studies

INTRODUCTION

The pseudo-continuous arterial spin labeling (pCASL) technique imitates continuous arterial spin labeling (CASL) by applying a train of short radiofrequency (RF)

pulses in rapid succession (1). To match the phase evolution of the flowing spins during labeling, a theoretical interpulse phase increment ($\Delta\phi_{th,L}$) is applied:

$$\Delta\phi_{th,L} = \gamma G_{mean} \Delta z \Delta t, \quad [1]$$

where γ is the gyromagnetic ratio, G_{mean} is the mean gradient, Δz is the labeling slice offset, and Δt is the time interval between two pCASL RF pulses. Two different gradient schemes have been proposed for the control experiment (2): balanced pCASL, with similar mean gradient for label and control conditions, and unbalanced pCASL, with null mean gradient during control. For standard pCASL measurements, the unbalanced method is recommended (3,4), as it is known to be less sensitive to off-resonance effects (2). The theoretical interpulse phase increment during control ($\Delta\phi_{th,C}$) is shifted by 180° relative to the one used in the label condition to avoid labeling. For unbalanced pCASL, because the mean gradient is zero, $\Delta\phi_{th,C} = 180^\circ$.

At higher magnetic fields, B_0 inhomogeneities in the labeling plane, away from the isocenter, increase and affect the spins' phase. Therefore, the theoretical interpulse phase increments $\Delta\phi_{th,L}$ and $\Delta\phi_{th,C}$ may not be optimal anymore. In this condition, arterial blood magnetization may not be fully inverted during labeling and some inversion may occur during control. Altogether, this lowers the inversion efficiency (IE) and the relative ASL signal, yields unstable ASL signals across subjects, and leads to interhemispheric asymmetry, as previously reported (5–9).

Placing the labeling plane at the isocenter is a way to obtain high IE (4), but at the cost of image quality, as the readout is not located at the isocenter anymore. Several correction strategies were developed for balanced pCASL. In multiphase pCASL (10,11), images with different pCASL phase offsets are acquired and are fitted to a model to retrieve the CBF. However, this method is based on a blood velocity dependent model and yields a lower signal-to-noise ratio per unit of time. Jahanian et al (12) presented a field-map-based approach at 3 T: The mean gradient and RF phase are corrected based on the measurement of the off-resonance field and gradient. However, at higher magnetic field, it can become challenging to obtain accurate B_0 maps in areas away from the isocenter and where the magnetic field is heterogeneous. Luh et al (13) demonstrated for balanced pCASL on humans at 7 T, that varying the phase during a prescan to measure the optimal phase increment was a robust way to improve the overall perfusion signal while keeping the imaging plane close to the

¹Université Grenoble Alpes, Grenoble Institut des Neurosciences, Grenoble, France.

²Inserm, Grenoble, France.

³Bruker Biospin, Ettlingen, Germany.

*Correspondence to: Emmanuel L. Barbier, Ph.D., Grenoble Institut Des Neurosciences, Chemin Fortuné Ferrini, 38700 La Tronche, France. Tel: +33-4-56-52-05-88; Fax: +33-4-56-52-05-98; E-mail: emmanuel.barbier@univ-grenoble-alpes.fr.

Lydiane Hirschler, Clément Debacker, Sascha Köhler and Jérôme Voiron were paid by Bruker [CIFRE stipend to L.H. and C.D.].

The MRI facility IRMaGe is partly funded by the French program "Investissement d'Avenir" run by the French National Research Agency (grant "Infrastructure d'avenir en Biologie Sante" [ANR-11-INBS-0006]).

Received 9 December 2016; revised 3 May 2017; accepted 4 May 2017

DOI 10.1002/mrm.26767

Published online 6 June 2017 in Wiley Online Library (wileyonlinelibrary.com).

isocenter. Moreover, other studies showed that correcting the control condition separately improves the ASL signal (14,15). However, the latter control correction strategies resulted in applying different frequencies for the label and the control conditions, leading to residual magnetization-transfer effects. Even if these residual effects may be negligible for magnetic fields up to 4 T, they are much more pronounced at high magnetic fields, and may therefore bias the ASL signal.

Here, we investigated a phase-optimization prescan approach for unbalanced pCASL on rats at 9.4 T. We analyzed the effect of separately optimizing the label and the control interpulse phases on the relative ASL signal and on its interhemispherical symmetry. We challenged the robustness of this phase-correction approach by manually changing the shims. In a second step, the dependence of the obtained optimized phase values on the shim settings and on the Larmor frequency at the location of the carotids in the labeling plane was evaluated.

THEORY

The presence of an off-resonance frequency offset Δf introduces an additional phase accumulation of $2\pi \Delta f \cdot \Delta t$ in between two successive pCASL RF pulses and shifts the real tagging location by $-2\pi \Delta f / (\gamma G_{max})$, where G_{max} is the gradient applied during the RF pulse. Altogether, when adding these modifications to Equation [1], the expected total interpulse phase to apply is

$$\Delta\phi = \gamma G_{mean} \left(\Delta z - \frac{2\pi \Delta f}{\gamma G_{max}} \right) \Delta t + 2\pi \Delta f \cdot \Delta t. \quad [2]$$

As a consequence, the phase correction $\Delta\phi_{corr}$ to add to the theoretical phase $\Delta\phi_{th}$ should be

$$\Delta\phi_{corr} = 2\pi \Delta f \cdot \Delta t \left(1 - \frac{G_{mean}}{G_{max}} \right). \quad [3]$$

For the control condition, because G_{mean} is 0 mT/m, the expected control-phase correction $\Delta\phi_{corr,C}$ is $2\pi \Delta f \cdot \Delta t$.

In the following, these theoretical interpulse phases obtained in presence of a frequency offset at the labeling plane are compared with the experimentally measured values.

METHODS

Animals

A total of 21 healthy rats (Sprague-Dawley male rats, 6–8 weeks old, weight: 200–300 g, Charles Rivers, France) were used. All experiments were approved by the local ethics committee and were performed in compliance with the guidelines of the European community (EUVD 86/609/EEC) for the care and use of the laboratory animals. Experiments were performed under permits (No. 380945 for E.B., A3851610008 for animal facilities) from the French Ministry of Agriculture. All procedures were performed under isoflurane anesthesia (IsoFlo, Axience, France, 5% for induction, 2% for maintenance). Respiration rate, heart rate, oxygen saturation, and rectal temperature were monitored and maintained within the

following ranges: 40–60 breaths/min, 400–500 beats/min, 98–100%, and 36–37°C, respectively.

Magnetic Resonance Sequences

Experiments were performed on a 9.4T horizontal scanner (Avance III-HD, Bruker BioSpec, Ettlingen, Germany; IRMaGe MRI facility, La Tronche, France) with a quadrature volume transmit and a phased-array surface receive coil configuration.

We first detail all MR sequences that were used in this study and describe the protocols in a separate subsection (“Experimental Protocols”).

Echo-Planar Imaging

All echo-planar imaging (EPI) based sequences (i.e., ASL and T_1 maps) were acquired with the following readout parameters: single-shot spin-echo EPI, echo time (TE)/repetition time (TR) = 22/4000 ms (unless mentioned otherwise), in-plane resolution = $234 \times 234 \mu\text{m}^2$, one 1-mm thick slice.

Labeling

Unless mentioned otherwise, unbalanced pCASL was applied in the rat’s neck (at $\Delta z = -2$ cm from the isocenter) during $\tau = 3$ s followed by a 300-ms postlabeling delay (ω). The labeling pulse train consisted of 400- μs Hanning-window-shaped RF pulses repeated every 800 μs and scaled to an average B_1 amplitude of 5 μT during the RF pulse train. G_{max}/G_{mean} were set to 45/5 mT/m.

The following sequences were used in this study, but not all for each animal (see “Experimental Protocols” subsection for more details):

- **Anatomical T_2 -weighted (T_{2w}) images** were obtained through a spin-echo sequence (TR/TE = 3346/33 ms, resolution = $0.137 \times 0.137 \times 0.8 \text{ mm}^3$, number of averages (NA) = 2, acquisition time (T_{acq}) = 3 min 34 s).
- A **T_1 map** was acquired for cerebral blood flow (CBF) quantification (16) using a nonselective inversion recovery sequence (TR/TE = 10000/19 ms, 18 inversion times (TIs) between 30 and 10000 ms, T_{acq} = 4 min). Other EPI parameters were identical to the aforementioned ones.
- **Label-phase optimization prescan** (T_{acq} = 100 s). During this scan, perfusion images were measured with the previously described EPI readout and pCASL-labeling parameters, except that the labeling duration was reduced to 1.5 s and the slice thickness was set to 4 mm (single slice, TR = 2 s). To quickly measure the labeling efficiency and to characterize interhemispheric asymmetry, relative cerebral perfusion weighted EPI images were acquired. A total of 25 label-control pairs, each with a different label interpulse phase, were obtained: the phase was swept from 0° correction ($\Delta\phi_{th,L} + 0^\circ$) to 360° correction ($\Delta\phi_{th,L} + 360^\circ$) with a 15° step. The interpulse phase increment of the control experiment was set to 180° ($\Delta\phi_{th,C}$). From this scan, the label interpulse phase correction $\Delta\phi_{corr,L}$ was extracted (see “Data Processing” subsection).

- **Control-phase optimization prescan** ($T_{acq} = 100$ s). This time, the label-phase increment was fixed to the optimized label-phase increment ($\Delta\phi_{th,L} + \Delta\phi_{corr,L}$), and the control interpulse phase increment was swept from 0° correction ($\Delta\phi_{th,C} + 0^\circ$) to 360° correction ($\Delta\phi_{th,C} + 360^\circ$) with a 15° step. All other parameters were the same as for the label-phase prescan. From this scan, the control interpulse phase correction $\Delta\phi_{corr,C}$ was extracted.
- **pCASL perfusion scan** ($T_{acq} = 4$ min): 30 label-control pairs of pCASL-EPI experiments were acquired with the previously described labeling and EPI parameters. The label-phase and control-phase increments were set as described in the experimental protocol.
- **Magnetization-transfer-corrected CASL-EPI scans** were acquired with the previously described EPI parameters. The labeling parameters were the same as for the pCASL sequence except that the labeling gradient was set to 10 mT/m. To correct for the asymmetrical spectrum of the macromolecules, the control frequency of the CASL experiment was optimized before the CASL-EPI acquisition, as described in (17).
- **Inversion efficiency** values were measured 5 mm downstream of the labeling plane for CBF quantification with a flow-compensated gradient-echo sequence (TR/TE = 225/5.6 ms, resolution = 0.117×0.117 mm², 1-mm slice thickness, NA = 2, $T_{acq} = 3$ min 30 s). Sequence-specific labeling parameters were: $\tau = 200$ ms and $\omega = 0$ ms (other labeling parameters were the same as that of the pCASL).
- The water frequency along the carotids was measured by means of a **PRESS sequence** with outer volume suppression and without water-suppression module: $2 \times 2 \times 2$ mm³ voxel size, TR = 2500 ms, TE = 13 ms, NA = 12, $T_{acq} = 30$ s.

Data Processing

The MRI data were analyzed using software developed in-house in MATLAB (The MathWorks Inc, Natick, MA).

T_1 maps were obtained by fitting the following equation to the signal from each pixel using a Levenberg-Marquardt algorithm:

$$M_z(TI) = M_0 \cdot (1 - 2\kappa e^{-TI/T_1}), \quad [4]$$

where $M_z(TI)$ is the MR signal collected at each TI, M_0 is the magnetization at thermal equilibrium, T_1 is the longitudinal relaxation time constant of tissue, and κ is the inversion efficiency.

The IE was derived from a complex reconstruction of the (p)CASL-FcFLASH sequence as follows:

$$IE = \left| \frac{M_C - M_L}{2M_C} \right|, \quad [5]$$

where M_C and M_L are the complex signals from the control and the label experiments, respectively. A region of interest was manually drawn on each carotid. The IE was obtained as the mean IE across both carotids.

To derive the phase correction, the regions of interest were manually drawn to delineate the left and right brain hemispheres (Fig. 1f). The relative perfusion signal in both hemispheres ($rASL_{left}$ and $rASL_{right}$) (in percent) was calculated as

$$rASL = \frac{\Delta M}{M_C} * 100, \quad [6]$$

where ΔM is the magnitude difference between control and label acquisitions, and M_C is the magnitude signal from the control experiment. $rASL_{left}$ and $rASL_{right}$ were plotted as a function of the label (resp. control) phase values; $\Delta\phi_{corr,L}$ was determined by visual inspection to be the center of the plateau yielding close to maximal $rASL$ on the label-phase optimization graph (Fig. 1b); and $\Delta\phi_{corr,C}$ was defined as the phase that is the furthest away from the dip of the control-phase optimization graph: control minimum + 180° (Fig. 1c).

To evaluate the quality of the phase optimization, the mean ($rASL_{mean}$) and the difference in ASL signal magnitude between hemispheres ($rASL_{asymmetry}$) were computed as

$$rASL_{asymmetry} = \frac{|rASL_{left} - rASL_{right}|}{|rASL_{left}| + |rASL_{right}|} * 100 \quad [7]$$

$$rASL_{mean} = \frac{|rASL_{left} + rASL_{right}|}{2}. \quad [8]$$

To calculate quantitative CBF maps, we assumed a single compartment and used the standard kinetic model developed by Buxton et al (18). Assuming that the arterial transit time is equal to the postlabeling delay, and that M_0^b , the magnetization of arterial blood at thermal equilibrium, may be approximated by M_0^t/λ , where M_0^t is the magnetization of tissue at thermal equilibrium and λ the blood-brain partition coefficient of water (0.9 mL/g) (19), we used the following equation pixel-by-pixel to quantify CBF (mL/100 g/min) (3,16,18):

$$CBF = \frac{6000 \cdot \lambda \cdot \Delta M \cdot \exp(\omega/T_1^b)}{2 IE \cdot T_1^t \cdot M_0^t \cdot (1 - \exp(-\tau/T_1^t))}, \quad [9]$$

where ΔM is the signal difference between control and label acquisitions averaged over repetitions; T_1^t is the apparent T_1 of tissue from the T_1 map; T_1^b is the longitudinal relaxation time of blood (2430 ms at 9.4 T) (20–22); and M_0^t is the control image intensity of the ASL experiment multiplied by $[1 - \exp(-TR/T_1^t)]^{-1}$ to correct for incomplete T_1 relaxation during the 4-s TR.

Experimental Protocols

Experiment 1

This experiment ($n = 8$ animals) was designed to evaluate the effect of correcting label and/or control interpulse phase increments on the perfusion signal. The following MR scans were performed with axial slice orientation after a standard global first-order shim (called “study shim”) (the details of each sequence are provided in the “Magnetic Resonance Sequences” subsection):

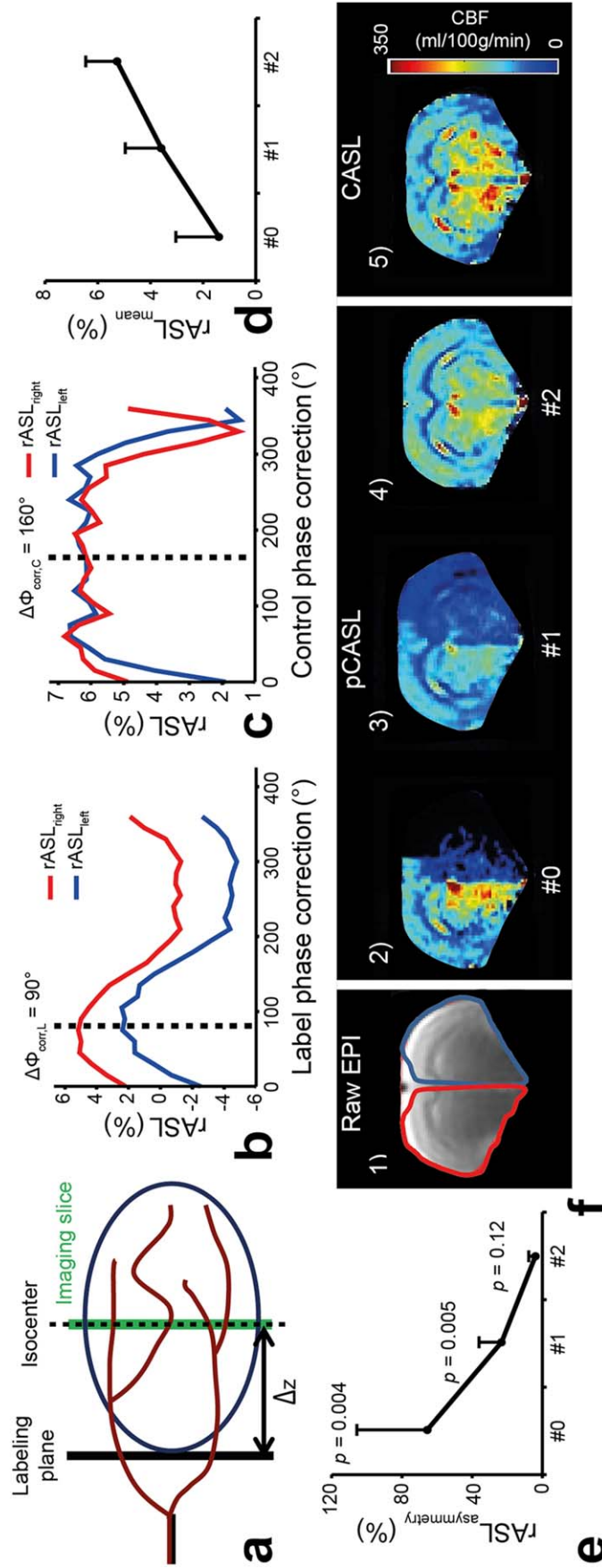


FIG. 1. Phase-correction strategy with prescans. **a**: Setup illustration. **b**: Example of a label-phase optimization graph for one animal: rASL_{left} (blue) and rASL_{right} (red) as a function of the additional phase increment. Left and right hemispheres were delineated as shown on the raw EPI image **f**. $\Delta\Phi_{corr,L}$ and $\Delta\Phi_{corr,C}$ are the optimized phase corrections for this particular animal. **d**: Relative ASL signal across eight animals; #0, no correction; #1, label-phase correction only; #2, label- and control-phase corrections. **e**: Asymmetry between hemispheres for eight animals; p indicates the result of a paired t-test for left/right hemisphere comparison. **f**: Quantitative CBF maps from the same animal as in **b** and **c**: (1) raw EPI image with left (blue) and right (red) delineated hemispheres; (2) pCASL without correction #0; (3) pCASL with label-phase correction only #1; (4) pCASL with label- and control-phase corrections #2; (5) CASL. Negative values are represented in black (e.g., right hemisphere in panel **f**, 2). Data expressed as mean \pm SD.

1. **Anatomical T_{2w} scan;**
2. **T_1 map;**
3. **Label and control optimization prescans**, from which the label and control interpulse phase corrections ($\Delta\phi_{\text{corr,L}}$ and $\Delta\phi_{\text{corr,C}}$, respectively) were extracted;
4. **Three pCASL-EPI perfusion scans:** one without any phase optimization (#0, using $\Delta\phi_{\text{th,L}}$ and $\Delta\phi_{\text{th,C}}$), one with an optimized label-phase increment and a theoretical control-phase increment (#1, using $\Delta\phi_{\text{th,L}} + \Delta\phi_{\text{corr,L}}$ and $\Delta\phi_{\text{th,C}}$), and one with both optimized label and control phase increments (#2, using $\Delta\phi_{\text{th,L}} + \Delta\phi_{\text{corr,L}}$ and $\Delta\phi_{\text{th,C}} + \Delta\phi_{\text{corr,C}}$);
5. A **CASL-EPI** perfusion scan, acquired in a subset of animals ($n=5$) to compare with the pCASL experiments. This sequence was chosen because the IE of CASL is not as sensitive to B_0 inhomogeneities as that of pCASL; and
6. **Inversion efficiency**, which was measured for CBF quantification both for CASL and pCASL without optimized phases and with an optimized label phase. The IE values with both optimized label and control phases for pCASL were measured separately in three animals.

Experiment 2

This experiment ($n=5$ animals) was designed to evaluate the robustness of the phase optimization in the presence of different magnetic field distributions, and to evaluate its limits. Field inhomogeneity was changed in a controlled fashion by modifying study shim values manually to introduce asymmetry between carotids, to change the frequency profile along the vessels, and to evaluate the effect of second-order shims, which may often be necessary to optimize image quality. We explored shim amplitudes up to the maximum shim values that still allowed sufficient image quality for the analysis (i.e., up to four times the study shim values). The shims were changed as follows:

- The average \pm standard deviation (SD) shim values across five animals were X (34 ± 91) Hz/cm, Y (-312 ± 277) Hz/cm, Z (610 ± 545) Hz/cm, and $Z^2 = 0$ Hz/cm²;
- The initial X (left–right direction) shim value was multiplied by -2 , 0 , 2 , and 4 (max = 233 Hz/cm, min = -116 Hz/cm). These shim conditions were called $-2X$, $0X$, $2X$, and $4X$;
- The Y (ventro–dorsal direction) shim value was multiplied by 2 , 1.5 , 0.5 , and 0 (max = 0 Hz/cm, min = -784 Hz/cm). These shim conditions were called $2Y$, $1.5Y$, $0.5Y$, and $0Y$;
- The initial Z (head–foot direction) shim value was multiplied by 2 , 1.5 , 0.5 , and 0 (max = 1626 Hz/cm, min = 0 Hz/cm). These shim conditions were called $2Z$, $1.5Z$, $0.5Z$, and $0Z$; and
- Four different values for the Z^2 shim were applied between -300 (called $-2Z^2$) and 300 ($2Z^2$) Hz/cm². These values are in the range of values obtained after a second-order shim on the rat brain in our system.

Shims were changed one at a time; the other values were set to the initial study shim values. Label- and

control-phase optimization prescans were acquired for each shim situation. From the label-phase optimization graph, $\Delta\phi_{\text{corr,L}}$ and the relative perfusion value without any phase optimization were extracted (#0). $\Delta\phi_{\text{corr,C}}$ and the relative ASL signal with both optimized phases (#2) were obtained from the control-phase optimization graph. The relative ASL signal with the optimized label phase only (#1) was obtained from both label- and control-optimization graphs, and the reported value is the average of both extracted values.

Experiment 3

To evaluate the dependence of the optimized phase value on the resonance frequency measured at and around the labeling plane (12), the following two experiments were performed:

1. In a first group of animals ($n=3$), frequency profiles were measured along each carotid, and the optimized label and control phases were derived after a second-order shim and in 11 additional Z-shim conditions: First, the Z-shim component was modified to null the observed gradient along the carotids, measured over 4 mm (cf. simulations) around the labeling plane. From this nulled gradient condition, -1000 to $+1000$ Hz/cm with a 200-Hz/cm step were added to the Z-shim. Profiles were measured with the PRESS sequence at 13 positions between $z = -25$ mm and -10 mm. From the obtained frequency profiles, the gradient around the labeling plane was derived (linear fit over 4 mm), and the frequency at -20 mm was retrieved. The data from the phase-optimization graphs were fitted to an ad hoc model, in which the phase of the maximum signal, the duty cycle, the transition width, and the signal amplitude were the estimated parameters; and
2. For a second group of animals ($n=5$), we optimized the label and control interpulse phases with the prescans, and measured the frequency with the PRESS sequence in both carotids at the labeling plane. An IE scan was acquired using optimized label and control phases. This entire experiment was performed using a global first-order shim and a local (brain) second-order shim.

Simulations

To evaluate the distance over which the inversion of arterial blood magnetization occurs and to confirm the label- and control-phase dependence on frequency, a moving magnetization vector in the presence of a pCASL sequence was simulated in MATLAB and followed while crossing the labeling plane. Bloch equations were integrated with a step size of $1 \mu\text{s}$. Parameters for the pCASL labeling were identical to the ones used in vivo, except for the labeling duration, which was set to 200 ms. The blood-flow velocity was set to the average blood velocity in the rat's carotids (i.e., 10 cm/s) (23). The inversion distance was measured as the distance over which the magnetization varies from 0.5% to maximum inversion.

Phase-optimization experiments were simulated by repeating the inversion simulation for different RF interpulse phase increments. The longitudinal magnetization intensity after inversion was retrieved and plotted against the applied interpulse phase increment to determine the phase that yields the best inversion. Such simulated phase-optimization experiments were also performed when the resonance frequency of the spins was offset with respect to the RF carrier.

Statistical Analysis

Paired t-tests were performed to evaluate the difference in ASL signal between hemispheres, and to compare quantitative CBF values obtained from the phase-optimized pCASL with the ones from the CASL experiment. A value of $P < 0.01$ was considered significant. All data are expressed as mean \pm SD.

RESULTS

Experiment 1

An example of a phase-optimization experiment is shown in Figure 1: rASL is drawn as a function of the interpulse phase-increment correction for label (Fig. 1a) and control (Fig. 1b) experiments. For this particular rat, the interpulse phase needed a correction of 90° for labeling and 160° for control. As these corrections differed among rats, $\Delta\phi_{\text{corr,L}}$ and $\Delta\phi_{\text{corr,C}}$ were measured for each animal. The relative perfusion signal $\text{rASL}_{\text{mean}}$ improves when applying the optimized phases (Fig. 1d and 1f): Optimizing the label phase increases the ASL signal by more than a factor of 2 ($\text{rASL}_{\text{mean}} = 1.4 \pm 1.7\%$ without correction and $3.6 \pm 1.4\%$ with an optimized label phase). When adding an optimized control phase, another 50% increase is gained ($\text{rASL}_{\text{mean}} = 5.3 \pm 1.2\%$ with both optimized phases). Without any optimization, $\text{rASL}_{\text{mean}}$ is lower than the SD across rats (Fig. 1d), meaning that the perfusion measurement is very unstable. These intersubject variations are reduced when applying the optimized label and control phases.

If no optimization is performed or only the label phase is optimized, the ASL signal differs significantly between hemispheres (Fig. 1e), as determined by a paired t-test (#0 $P = 0.004$, #1 $P = 0.005$). This asymmetry is reduced to $4 \pm 3\%$ when both label and control phases are optimized (#2 $P = 0.12$).

We compared the quantitative CBF maps obtained with pCASL for each labeling condition (Fig. 1f, 2–4) to a CASL acquisition performed on the same animal during the same MRI session (Fig. 1f, 5). When only one or no phase is optimized, quantitative CBF maps obtained via pCASL are significantly different from the ones obtained with the CASL sequence (paired t-test for CASL versus pCASL #0: $P = 0.001$, CASL versus pCASL #1: $P = 0.006$). If both label and control phases are optimized (Fig. 1f, 4), pCASL scans yield CBF maps comparable to those from CASL (paired t-test CASL versus pCASL #2: $P = 0.21$). Remaining differences between CASL and pCASL ($-4 \pm 6\%$ relative change) may be ascribed to physiological fluctuations in perfusion. For the animal shown in Figure 1f, the CASL scan was acquired 13 min

after the pCASL scan, which can explain the observed CBF variations. Still, the observed contrast on both CASL and pCASL (#2) CBF maps is similar, with higher cortical and thalamic perfusion values compared with white-matter CBF (corpus callosum). The average brain CBF (from #2 pCASL) was $153 \pm 25 \text{ mL}/100\text{g}/\text{min}$, which is comparable to values from literature obtained in Sprague-Dawley rats under isoflurane anesthesia (24–27).

This experiment shows that optimizing both label and control phases dramatically improves relative perfusion signal obtained with unbalanced pCASL, corrects asymmetry arising when labeling far from the isocenter at high field, and preserves high image quality at the same time.

Experiment 2

This experiment investigated the robustness of the phase optimization to different magnetic field inhomogeneities. Figure 2a shows the difference between the measured left and right optimized label-phase values for all shim conditions. As expected, when increasing the frequency difference between carotids (i.e., changing the X-shim), asymmetry arises in $\Delta\phi_{\text{corr,L}}$ as well. However, for all situations, optimizing both label and control phases leads to maximum and stable ASL signal (Fig. 2b), with minimal signal loss at degraded x-shims, whereas without any optimization or only an optimized label phase, the ASL signal is lower and unstable. The asymmetry observed in absence of optimized phases was reduced to $1 \pm 3\%$ when performing both optimizations in all shim conditions (Fig. 2c) (i.e., up to four times the observed study shim values).

Experiment 3

We evaluated the relation between the frequency profile around the labeling plane and the optimized phase values. According to our simulations, inversion occurs over a distance of 3.8 mm (represented as a gray band on Figs. 3a–3c). Varying the Z-shim changes the gradient around the labeling plane, the frequency at the labeling plane, and the label and control phase optimization graphs (Fig. 3). Figures 4a and 4b show that the phase-correction values are strongly correlated to the frequency measured at the center of the labeling plane. A small difference can be observed between the expected and measured phase values, leading to a slope of the linear fit approximately 11% smaller than expected. Figure 4c and 4d show that this phase difference (noted “residual $\Delta\phi_{\text{corr}}$ ”) does not depend on the gradient around the labeling plane. This gradient, however, slightly affects the duty cycle of the label-phase optimization graph (Figs. 4e and 4f). This duty cycle is independent of the frequency at the labeling plane (data not shown). Figures 4g and 4h show that the rASL signal amplitude becomes less dependent on the gradient around the labeling plane when both corrections are performed.

To further explore the dependence of optimized phase increments on the resonance frequency at the labeling plane under standard imaging conditions, Figure 5 shows data obtained using first- and second-order shims

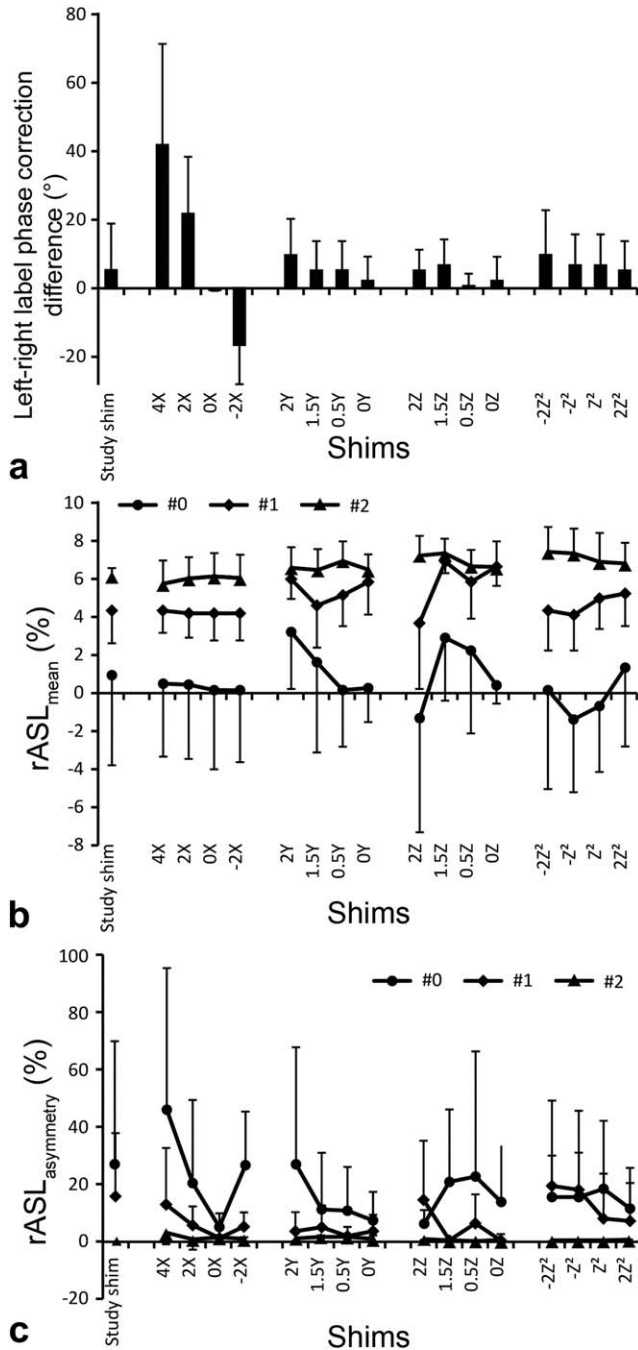


FIG. 2. Effect of phase correction on perfusion signal for different shim conditions (five animals). **a**: Left-right label-phase correction difference across shims. **b**: Relative perfusion signal. **c**: Asymmetry across hemispheres without phase correction (#0), with label-phase correction only (#1), and with both label- and control-phase corrections (#2). Data expressed as mean \pm SD.

optimized for imaging. Whether a first or a second-order shim is performed, the optimized phases $\Delta\phi_{\text{corr,L}}$ and $\Delta\phi_{\text{corr,C}}$ are strongly linearly correlated to the frequency f at the labeling plane (Fig. 5) as predicted by Equation [3]: The slope of the linear relation between $\Delta\phi_{\text{corr,L}}$ and the resonance frequency is now $0.26^\circ/\text{Hz}$ (i.e., $(1 - G_{\text{mean}}/G_{\text{max}})\Delta t \cdot 360$, as expected); for control, $\Delta\phi_{\text{corr,C}}$ is linearly related to f with a slope of $0.29^\circ/\text{Hz}$ ($=\Delta t \cdot 360$).

The simulated phase-optimization experiments confirmed these results (data not shown).

Unexpected offsets of the curves, however, are observed in vivo: At 0 Hz (no off-resonance effect), one would expect no need for phase correction; instead, a correction of 58° is required for labeling (offset_L) and 122° for control (offset_C). These offsets are stable across animals: The results shown in Figure 5 originate from five animals and match those observed in Experiment 3a.

For all five animals, after both label and control phase optimizations, IE was at $89 \pm 2\%$ and remained stable whether a second-order shim was performed or not; the IE difference between first- versus second-order shim was $0 \pm 3\%$.

DISCUSSION

In this study, we described and evaluated a method to obtain stable pCASL perfusion maps in rats at 9.4 T using unbalanced pCASL. Optimizing both label and control phases of unbalanced pCASL by means of prescans yields robust ASL signal, and the obtained quantitative CBF maps are comparable to those from CASL, a method less sensitive to B_0 inhomogeneities. Optimized phase values vary across animals and depend on shim parameters; therefore, it appears necessary to measure $\Delta\phi_{\text{corr,L}}$ and $\Delta\phi_{\text{corr,C}}$ for each animal. Applying a separate control phase correction (i.e., applying not necessarily the same $\Delta\phi_{\text{corr,C}}$ as $\Delta\phi_{\text{corr,L}}$) further improves the ASL signal and yields stable results across large shim and frequency ranges (i.e., up to 1000 Hz). Perfusion asymmetry between hemispheres, which could be as high as 100% without phase optimization, could be corrected with the proposed workflow, down to $1 \pm 3\%$ (mean \pm SD value for Experiments 1 and 2).

Each proposed prescan acquisition lasts 100 s. Data processing involves extracting the brain-average ASL signal as a function of RF phase increment, and determining the optimized phases, which is easily performed using simple offline tools. In total, the proposed optimization adds approximately 5 min to ASL protocols, which is acceptable in most preclinical animal studies.

Accounting for the loss in the inversion efficiency when quantifying the CBF values should yield constant CBF, in theory. However, we observed global CBF to be $66 \pm 68 \text{ mL}/100\text{g}/\text{min}$ in our group of animals ($n=8$) without correction, $105 \pm 40 \text{ mL}/100\text{g}/\text{min}$ with a label correction only, and $153 \pm 25 \text{ mL}/100\text{g}/\text{min}$ with both corrections. According to common practice, IE is calculated using Equation [5], leading to an always positive value, even when the ASL signal, and hence the actual IE, is negative. In case of negative IE in one or both carotids, the actual mean IE is overestimated, leading to an underestimation of global CBF. Moreover, the contribution of each carotid to the perfusion is not necessarily equal in each brain region. Reliable CBF quantification may therefore only be obtained when the actual IE is positive and similar in both carotids (i.e., when both phases are optimized).

Varying the shim settings in Experiment 2 changed the labeling and image slice positions and thicknesses (less than 5% for labeling and 20% for imaging) and distorted

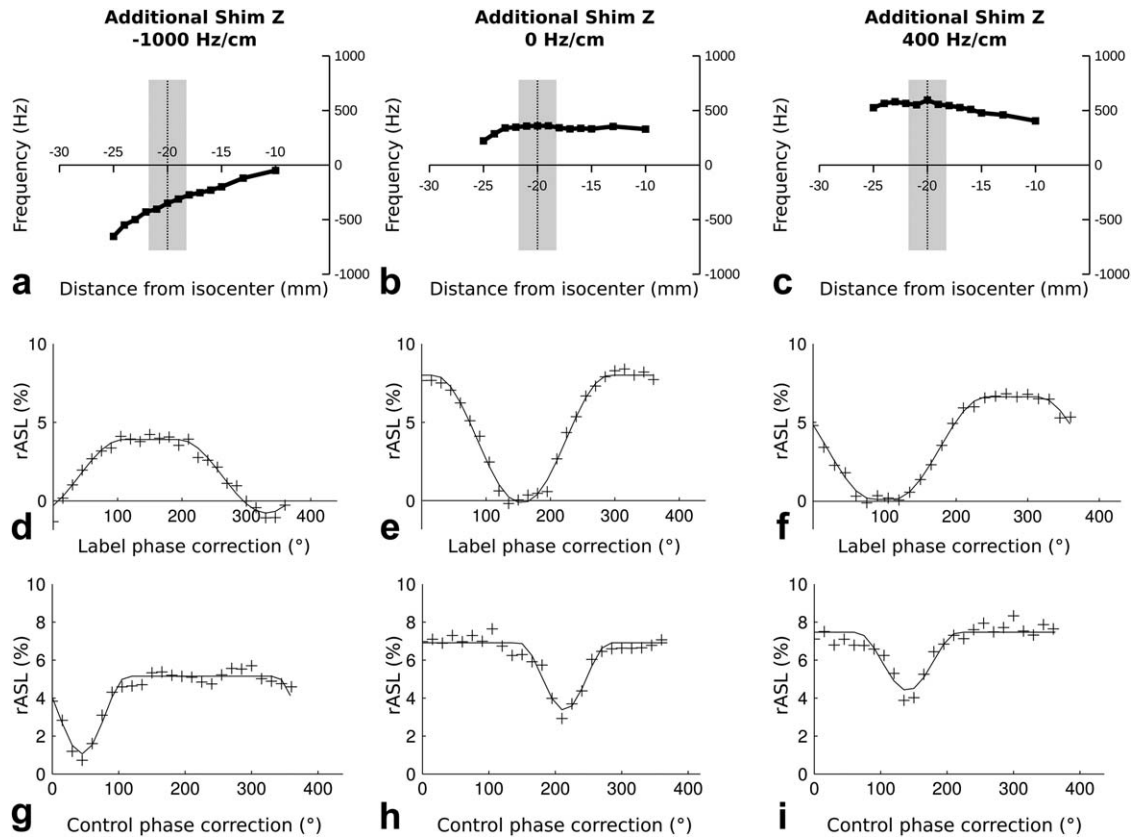


FIG. 3. Examples of frequency profiles along the left carotid for three shim conditions in one animal. From the situation with a compensated gradient around the labeling plane (b), additional Z-shims were added. Here we show two out of the 11 additional Z-shims: with an additional shim of -1000 Hz/cm (a) and 400 Hz/cm (c). Note that the actual additional gradient as measured with the PRESS sequence does not correspond to the nominal shim setting, suggesting an error in the shim unit conversion on our system. The labeling plane position is indicated by the black dashed lines, and the transition width, derived from the simulations, by the gray boxes. The label (d–f) and control (g–i) phase optimization graphs change depending on the shim condition. The full lines in (d–i) represent an ad hoc model fit to the data.

the images. This may have biased the ASL signal estimation and could have contributed to the variations of mean rASL values across shim settings (Fig. 2b). However, these variations were only moderate. The mean $rASL_{\text{mean}}$ for #2 across shim settings was $6.6 \pm 0.5\%$, a SD comparable to that obtained between animals for one shim setting. These residual variations in rASL between shims could also be caused by changes in perfusion, as the physiological status of the animal may have evolved during the experiment. Despite these variations, the fully optimized rASL signal (i.e., #2) is always higher than the nonoptimized ones (#0 and #1).

The measured phase corrections ($\Delta\phi_{\text{corr,L}}$ and $\Delta\phi_{\text{corr,C}}$) are strongly ($R^2 > 0.99$) correlated with the resonance frequency in the carotids at the labeling plane measured with the PRESS sequence. In Experiment 3a, under manually degraded shim conditions, both slopes differ from the expected ones (Eq. [3]). This is no longer true in Experiment 3b when shims optimized for imaging are used. This suggests that the slope difference observed in Experiment 3a may arise from shifts and/or distortions of the labeling and/or imaging planes. Note that the frequency ranges in both experiments are similar.

Figure 4 shows that the gradient around the labeling plane does not affect the optimized phase values, but

has a small effect on the duty cycle of the label-phase optimization graph. The blood velocity may also influence the shape of the phase optimization graph (28).

To further understand why a phase correction was needed in the absence of frequency offset at the labeling plane (Figs. 4a and 4b and Fig. 5), we evaluated the effect of different pCASL parameters on offset_L and offset_C by repeating Experiment 3b for different pulse spacing durations, maximum and mean gradients, and labeling slice positions. For all explored parameters, the curve's slope strictly followed Equation [3] (data not shown). The measured offset_L and offset_C , however, varied when changing the sequence parameters. This may stem either from sequence or from hardware issues, as the offsets stayed stable across animals for a given pCASL parameter set. To investigate the offsets' origin, pCASL gradient waveforms were measured on a water tube: By calculating the derivative of the MR signal phase difference between two slices over time while the pCASL gradients are played out, the effective gradient waveform can be obtained (29). These in situ gradient measurements confirmed that the effective average gradient seen by the spins is indeed following the pulse program's instructions. The phase shift resulting from imperfections in the gradient waveform was estimated to

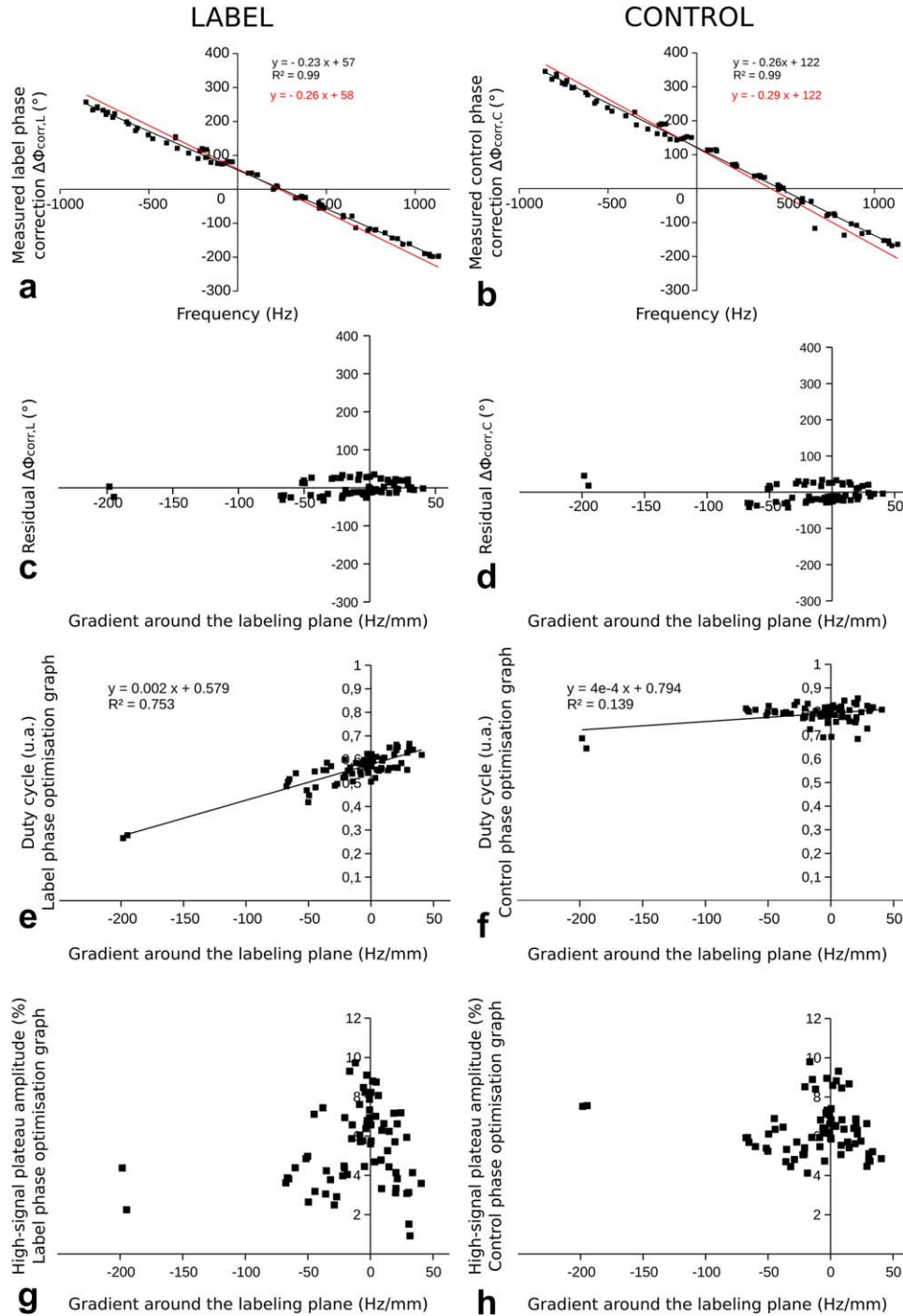


FIG. 4. Label (a) and control (b) phase corrections as a function of the resonance frequency measured at the labeling plane for all 12 shim conditions of Experiment 3a. Each data point corresponds to the optimized phase correction measured in one hemisphere and the frequency measured in the corresponding carotid, in one shim condition. The black line corresponds to the linear fit to the data, and the red line to the expected values. The slope of the red line was calculated according to Equation [3] and the offset was derived from Experiment 3b (cf. Fig. 5). c, d: Residual phase correction (i.e., the difference between the data points in (a) and (b) and the expected values). e, f: Dependence of the duty cycle of the label- and control-phase optimization graphs on the gradient around the labeling plane. The duty cycle was obtained as the proportion of the high-signal plateau (full-width half maximum) in the full phase cycle. g, h: Amplitude of the high-signal plateau, measured from the label- and control-phase optimization graphs, as a function of the gradient around the labeling plane. Note that, in one animal, the initial gradient around the labeling plane was much higher (~ 200 Hz/mm) than those observed in other animals.

be below 10° . Therefore, errors in gradient execution leading to large phase accumulation offsets may be excluded. The way the RF pulses are generated and played out from the pulse program may be another

possible explanation for the presence of the phase offsets. Indeed, depending on the way off-resonance RF pulses are produced, additional phase shifts appear (30). However, this could not be tested on our system with

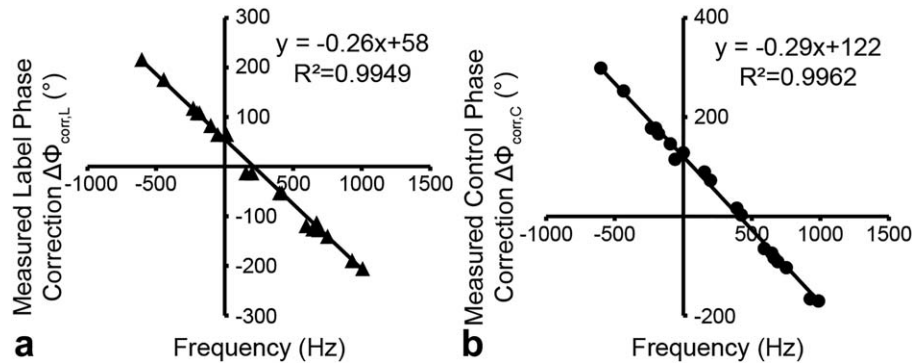


FIG. 5. Label- (a) and control-phase (b) corrections as a function of the resonance frequency measured at the labeling plane, located -20 mm from the isocenter. Each of the 20 data points corresponds to a phase correction measured in one hemisphere and a frequency measured in the corresponding carotid. The 20 data points result from the measurements in the two carotids of five animals under a first- and a second-order shim. All phase corrections were measured with a phase-optimization prescan. The equation corresponds to the linear fit to the data.

the current software. Such phase offsets could also be present on other MRI scanners developed by other companies.

Several improvements may be discussed. Combining the label and control phase optimization scans in one single acquisition is possible and would accelerate this adjustment step. Prediction of optimal phases from the frequency at the labeling plane is also an option. In the presence of additional hardware offsets as observed on our system, offset_L and offset_C have to be measured once for a particular set of pCASL parameters (e.g., labeling gradients, slice position, interpulse delay), and these values can then be combined with the frequency at the labeling plane measured in each animal to derive the required phase corrections. A phase correction based on the frequency measurement is particularly interesting for measuring perfusion in animals with low CBF: If the signal-to-noise ratio in the prescans becomes low, the optimal values of $\Delta\phi_{\text{corr,L}}$ and $\Delta\phi_{\text{corr,C}}$ may no longer be accurately detected.

If the difference between optimal label phases for the left and the right carotids is too large, a case not encountered in the present study despite strong shim changes, the proposed approach will no longer yield optimal pCASL labeling in both carotids. In these conditions, a dual-shim approach (i.e., application of different shim settings during labeling and during imaging) could be helpful in restoring a more homogeneous magnetic field at the labeling plane. Although dual shim alone did not seem sufficient to optimize pCASL in humans (9), combining this approach with the phase-optimization step should yield an optimal phase-correction value for both vessels, based on our results.

The phase optimization graphs in unbalanced pCASL differ between the label and control conditions, as a result of the difference in the pCASL gradient. This would not be observed in the case of balanced pCASL, for which the control optimization graph is a simple 180° shift in the label optimization graph. As the control-phase optimization graph has a high signal plateau larger than 180° , there always exists a joint optimized control phase for both carotids. This makes unbalanced pCASL more robust to B_0 inhomogeneities than balanced pCASL.

This study focused on the labeling of the blood flowing in the carotid arteries. When using the optimized label and control phases, the mean IE in the vertebral arteries across six animals was $74 \pm 7\%$, values smaller than those measured in the carotids for these animals ($90 \pm 1\%$, data not shown). To properly optimize the label and control phases specifically for the vertebral arteries, better knowledge of the vascular territories perfused by the vertebrales in rodents would be necessary. However, given the observed IE, and because vertebrales in rodents preferentially perfuse the cerebellum and much less the cerebral hemispheres (31), the proposed approach should provide near-optimal signal for most preclinical ASL studies.

In humans, carotid and vertebral arteries are separated by a greater distance and may therefore be subject to greater frequency differences. In this case, finding a compromise phase-correction value for all four arteries could be more difficult. A dual-shim approach could be helpful to restore a more homogeneous field at the labeling plane, permitting optimal phase-correction values for all vessels.

CONCLUSIONS

This study shows that performing both label- and control-phase corrections improves relative perfusion signal, corrects asymmetry arising when labeling far from isocenter at high field, and preserves high image quality at the same time. This correction approach yields stable results, also when the shim in the animal's neck is degraded, or if strong off-resonance effects are present. The phase-correction values are strongly correlated to the measured frequency in the carotids. The prediction of the phase correction from the frequency measurement in the carotids is therefore possible if offset_L and offset_C are known. Finally, in addition to the measurements presented in this work performed at 9.4 T, we successfully applied the label- and control-phase correction approach at ultrahigh field (17.2 T) (32) as well as on different scanners and animals (Pharmascan 7 T (33), BioSpec 11.7 T (34)). This approach is also expected to be beneficial for human studies

performed at high magnetic field, for which unbalanced pCASL is recommended (3).

ACKNOWLEDGMENTS

The authors acknowledge the excellent technical support of the MRI Facility of Grenoble (UMS IRMaGe), Franek Hennel for stimulating discussions, and Benjamin Lemasson for help with preparing the figures.

REFERENCES

- Dai W, Garcia D, De Bazelaire C, Alsop DC. Continuous flow-driven inversion for arterial spin labeling using pulsed radio frequency and gradient fields. *Magn Reson Med* 2008;60:1488–1497.
- Wu WC, Fernández-Seara M, Detre JA, Wehrli FW, Wang J. A theoretical and experimental investigation of the tagging efficiency of pseudocontinuous arterial spin labeling. *Magn Reson Med* 2007;58:1020–1027.
- Alsop DC, Detre JA, Golay X, et al. Recommended implementation of arterial spin-labeled perfusion MRI for clinical applications: a consensus of the ISMRM perfusion study group and the European consortium for ASL in dementia. *Magn Reson Med* 2014;116:102–116.
- Duhamel G, Callot V, Tachrount M, Alsop DC, Cozzone PJ. Pseudocontinuous arterial spin labeling at very high magnetic field (11.75 T) for high-resolution mouse brain perfusion imaging. *Magn Reson Med* 2012;67:1225–1236.
- Teeuwisse WM, Webb AG, Van Osch MJP. Arterial spin labeling at ultra-high field: all that glitters is not gold. *Int J Imaging Syst Technol* 2010;20:62–70.
- Ghariq E, Teeuwisse WM, Webb AG, Osch MJP Van. Feasibility of pseudocontinuous arterial spin labeling at 7 T with whole-brain coverage. *Magn Reson Mater Phys Bio. Med* 2012;25:83–93.
- Luh WM, Li TQ, Wong EC, Bandettini PA. Pseudo-continuous arterial spin labeling at 7 T. In Proceedings of the 16th Annual Meeting of ISMRM, Toronto, Canada, 2008. p. 3339.
- Hirschler L, Debacker CS, Voiron J, Warnking JM, Barbier EL. Robust inter-pulse phase correction for brain perfusion imaging at very high field using pCASL. In Proceedings of the 23rd Annual Meeting of ISMRM, Toronto, Canada, 2015. p. 2336.
- Teeuwisse WM, Schmid S, Helle M, van Osch MJP. 2-shim or not 2-shim, that is a question in pseudo continuous arterial spin labeling. In Proceedings of the 22nd Annual Meeting of ISMRM, Milan, Italy, 2014. p. 4808.
- Jung Y, Wong EC, Liu TT. Multiphase pseudocontinuous arterial spin labeling (MP-pCASL) for robust quantification of cerebral blood flow. *Magn Reson Med* 2010;64:799–810.
- Shin DD, Liu TT, Wong EC, Shankaranarayanan A, Jung Y. Pseudocontinuous arterial spin labeling with optimized tagging efficiency. *Magn Reson Med* 2012;68:1135–1144.
- Jahanian H, Noll DC, Hernandez-Garcia L. B₀ field inhomogeneity considerations in pseudo-continuous arterial spin labeling (pCASL): effects on tagging efficiency and correction strategy. *NMR Biomed* 2011;24:1202–1209.
- Luh WM, Talagala SL, Li TQ, Bandettini PA. Pseudo-continuous arterial spin labeling at 7 T for human brain: estimation and correction for off-resonance effects using a Prescan. *Magn Reson Med* 2013;69:402–410.
- Nezamzadeh M, Matson GB, Young K, Weiner MW, Schuff N. Improved pseudo-continuous arterial spin labeling for mapping brain perfusion. *J Magn Reson Imaging* 2010;31:1419–1427.
- Han PK, Choi SH, Park S. Investigation of control scans in pseudo-continuous arterial spin labeling (pCASL): strategies for improving sensitivity and reliability of pCASL. *Magn Reson Med* 2017;78:917–929.
- Debacker CS, Daoust A, Köhler S, Voiron J, Warnking JM, Barbier EL. Impact of tissue T₁ on perfusion measurement with arterial spin labeling. *Magn Reson Med* 2017;77:1656–1664.
- Barbier EL, Silva AC, Kim HJ, Williams DS, Koretsky AP. Perfusion analysis using dynamic arterial spin labeling (DASL). *Magn Reson Med* 1999;41:299–308.
- Buxton RB, Frank LR, Wong EC, Siewert B, Warach S, Edelman RR. A general kinetic model for quantitative perfusion imaging with arterial spin labeling. *Magn Reson Med* 1998;40:383–396.
- Herscovitch P, Raichle ME. What is the correct value for the brain—blood partition coefficient for water? *J Cereb Blood Flow Metab* 1985; 5:65–69.
- Nasrallah FA, Lee ELQ, Chuang K-H. Optimization of flow-sensitive alternating inversion recovery (FAIR) for perfusion functional MRI of rodent brain. *NMR Biomed* 2012;25:1209–1216.
- Dobre MC, Ugurbil K, Marjanska M. Determination of blood longitudinal relaxation time (T₁) at high magnetic field strengths. *Magn Reson Imaging* 2007;25:733–735.
- de Graaf RA, Brown PB, McIntyre S, Nixon TW, Behar KL, Rothman DL. High magnetic field water and metabolite proton T₁ and T₂ relaxation in rat brain in vivo. *Magn Reson Med* 2006;56:386–394.
- Kreis D, Schulz D, Stein M, Preuss M, Nestler U. Assessment of parameters influencing the blood flow velocities in cerebral arteries of the rat using ultrasonographic examination. *Neurol Res* 2011;33:389–395.
- Petrinovic MM, Hankov G, Schroeter A, Bruns A, Rudin M, von Kienlin M, Künnecke B, Mueggler T. A novel anesthesia regime enables neurofunctional studies and imaging genetics across mouse strains. *Sci Rep* 2016;6:24523.
- Kim T, Kim SG. Quantification of cerebral arterial blood volume and cerebral blood flow using MRI with modulation of tissue and vessel (MOTIVE) signals. *Magn Reson Med* 2005;54:333–342.
- Esparza-Coss E, Wosik J, Narayana PA. Perfusion in rat brain at 7 T with arterial spin labeling using FAIR-TrueFISP and QUIPSS. *Magn Reson Imaging* 2010;28:607–612.
- Hansen TD, Warner DS, Todd MM, Vust LJ, Trawick DC. Distribution of cerebral blood flow during halothane versus isoflurane anesthesia in rats. *Anesthesiology* 1988;69:332–337.
- Zhao L, Vidoreta M, Soman S, Detre JA, Alsop DC. Improving the robustness of pseudo-continuous arterial spin labeling to off-resonance and pulsatile flow velocity. *Magn Reson Med* 2017;78:1342–1351.
- Beaumont M, Lamalle L, Segebarth C, Barbier EL. Improved k-space trajectory measurement with signal shifting. *Magn Reson Med* 2007; 58:200–205.
- Hennel F. The effective phase of soft RF pulses. *Concepts Magn Reson* 2014;43A:127–137.
- Dorr A, Sled JG, Kabani N. Three-dimensional cerebral vasculature of the CBA mouse brain: a magnetic resonance imaging and micro computed tomography study. *NeuroImage* 2007;35:1409–1423.
- Ciobanu L, Hirschler L, Tsurugizawa T, Bihan D Le, Debacker C, Barbier EL. Cerebral perfusion measurements at 17.2 T using pCASL: a feasibility study. In Proceedings of the 23rd Annual Meeting of ISMRM, Toronto, Canada, 2015. p. 2964.
- Hirschler L, Munting LP, Teeuwisse WM, Suidgeest E, Warnking JM, Van Osch MJP, Barbier EL, van der Weerd L. Transit time mapping in the mouse brain using time-encoded pCASL. In: Proceedings of the 24th Annual Meeting of ISMRM, Singapore, Singapore, 2016. p. 4654.
- Debacker CS, Warnking JM, Koehler S, Voiron J, Barbier EL. Comparison of ASL inversion efficiency and CBF quantification for 3 perfusion techniques at 3 magnetic fields. In Proceedings of the 23rd Annual Meeting of ISMRM, Toronto, Canada, 2015. p. 794.